Arabian Journal of Chemistry (2021) **14**, 103057

King Saud University

**Arabian Journal of Chemistry**

www.ksu.edu.sa
www.sciencedirect.com

ORIGINAL ARTICLE

# Synthesis, biological evaluation, molecular docking and *in silico* ADMET screening studies of novel isoxazoline derivatives from acridone

**Mohammed Aarjane [a,*], Siham Slassi [a], Adib Ghaleb [b], Bouchra Tazi [c], Amina Amine [a]**

[a] *Laboratory of Chemistry/Biology Applied to the Environment, CMMBA, Faculty of Science, University Moulay Ismail, BP 11201 Zitoune, Meknes, Morocco*
[b] *Laboratory of Analytical and Molecular Chemistry, Multidisciplinary Faculty of Safi, Cadi Ayyad University, Safi, Morocco*
[c] *National School of Agriculture, Department of Basic Sciences, Meknes, Morocco*

Received 20 December 2020; accepted 29 January 2021
Available online 10 February 2021

**KEYWORDS**

Acridone;
Antibacterial evaluation;
Isoxazoline;
Molecular docking;
ADMET

**Abstract** A series of new acridone derivatives from isoxazoline (**2a-l**) were synthesized via 1,3-dipolar cycloaddition reaction between a variety of aryl nitrile oxides and N-allyl acridones using simple and efficient methods. This is the first ever green protocol to synthesize novel isoxazolines derivatives from acridone under microwave condition and offers broad substrate scope with good to excellent yields. The synthesized compounds (**2a-l**) were tested for their antibacterial potency against four pathogenic bacterial and were found to exhibit moderate to potent antibacterial activity. Two of these compounds **2a** and **2k** exhibited a significant antibacterial activity against *E. coli* and *P. putida,* respectively. The *in silico* molecular docking results supported the antibacterial activity of the synthesized compounds. ADMET properties of the most synthetized compounds showed an excellent bioavailability, therefore, can be considered as promising drugs candidates for further studies.


## 1. Introduction

Heterocycles compounds have served as valuable synthetic templates for the synthesis of new compounds with interesting biological properties (Jia et al., 2020). Antibacterial activities of heterocycles, particularly those with nitrogen and oxygen as heteroatoms are well documented in the literature (Aarjane et al., 2020c; Banerjee, 2017; Guariento et al., 2018; Naouri et al., 2020; Zorina et al., 2019). Among these heterocycles, acridones have attracted much attention as a result of their divers medicinal applications, including antimalarial (Kumar et al., 2009), antibacterial (Aarjane et al., 2019), anticancer (Oyedele et al., 2020), and anti-inflammatory (Sondhi et al., 2010) (Fig. 1). Moreover, the photophysic properties of acridones allow these kind of compounds to be interesting tools for selective recognition in ecological and biological areas

* Corresponding author.
E-mail address: m.aarjane@edu.umi.ac.ma (M. Aarjane).
Peer review under responsibility of King Saud University.

Production and hosting by Elsevier

https://doi.org/10.1016/j.arabjc.2021.103057
1878-5352 © 2021 Published by Elsevier B.V. on behalf of King Saud University.

(Aarjane et al., 2020b). On the other hand, isoxazolines are key skeletons of several synthetic and naturally occurring pharmacologically active compounds such as antitumor (Ribeiro et al., 2017), anti-HIV (Srivastava et al., 1999), antibacterial (Zghab et al., 2017) and anticancer (Kaur et al., 2014) (Fig. 1). Numerous methods have been reported for the preparation of these heterocycles, 1, 3-dipolar cycloaddition reactions are typically utilized to construct isoxazoline ring (Bonacorso et al., 2018; Dadiboyena and Nefzi, 2012; Rouf et al., 2017).

In recent years, antibiotic resistance has become a major problem to public health security worldwide (Yin et al., 2020) and the occurrence of antibiotic resistance has expected an alarming rate the world over (Botelho and Schulenburg, 2020). Some *P. putida* shows a high resistance phenotype to diverse xenobiotic and organic compounds such as flavonoids, β-lactam antibiotics and other antimicrobial compounds (Fernandez-Escamilla et al., 2015). The transcriptional regulator (TtgR) enzyme of *P. putida* is a HTH-type transcriptional repressor that controls expression of the TtgABC efflux pump, which is the main contributor to resistance against several antimicrobials agents in this bacteria (Terán et al., 2003). Moreover, previous studies on the TtgR multidrug binding potential have shown that it binds with moderate to high affinity to plant-derived compounds such as phloretin and naringenin (Alguel et al., 2007b; Choudhury, 2010). All of these compounds are characterized by having an aromatic ring (Daniels et al., 2010). On the other hand, MenB or dihydroxynaphthoic acid synthetase, is involved in the biosynthesis of menaquinone. *E. coli* utilize menaquinone (vitamin K2), a polyisoprenylated naphthoquinone, as the lipid-soluble redox cofactor in the electron transport chain of bacteria. The enzymes in the biosynthetic pathway of bacterial menaquinone are potential targets for novel antibacterial drug (Sharma et al., 1992). Several new scaffolds have been identified as dihydroxynaphthoic acid synthetase inhibitors (Amzoiu et al., 2020; Evans et al., 2016).

Computational tools in drug discovery become a major role in the development of therapeutically important small compounds (Franchini et al., 2017; Ragusa et al., 2017). These computational methods are relevant in limiting the use of animal models and for aiding the rational design of novel and safe drug candidates (Brogi et al., 2020; Righetti et al., 2020). The *in silico* molecular docking technique was applied to explain the obtained biological activities by identify the stable poses of synthesized compounds into the studied receptor pocket. During clinical drug development process many drugs candidates can be excluded due to pharmacokinetic problems which affect costs and time investments in drug discovery process (Ghaleb et al., 2020). To overcome this problem an *in silico* ADMET (Absorption; Distribution; Metabolism, Excretion and Toxicity) study was applied to predict drugs pharmacokinetics.

In view of the promising antibacterial profile of acridones as well as isoxazolines and also relying on our previous studies on acridone derivatives as potent antibacterial agents (Aarjane et al., 2020a), we have synthesized novel compounds of both isoxazoline and acridone pharmacophores, with the expectation of a synergetic effect. The adopted strategy for preparing novel isoxazoline derivatives from acridone was based on the 1,3-dipolar cycloaddition reaction between N-allyl acridone

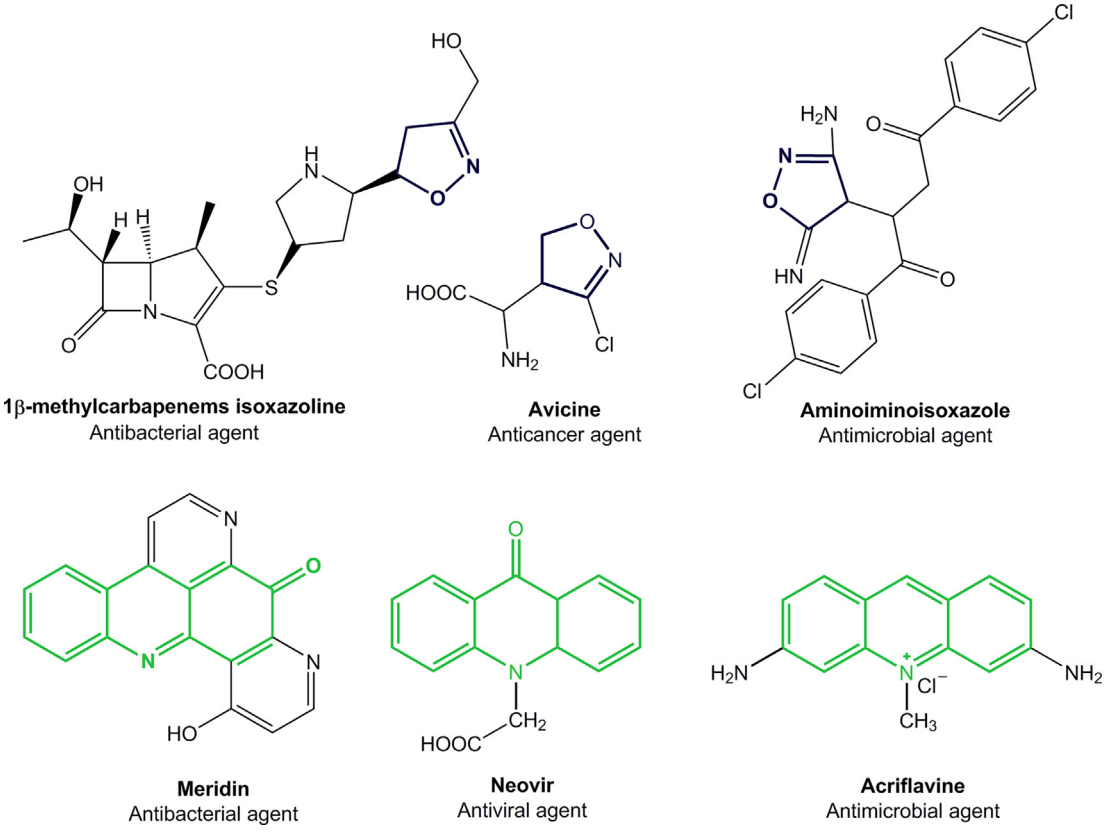


**Fig. 1** Isoxazolines and acridones used as pharmaceuticals agents.

and nitrile oxides using simple and efficient methods. The newly synthesized compounds were then tested for their potential antibacterial activities. Furthermore, molecular docking study have been applied to explain and identify the possible modes of interactions between synthesized compounds and studied receptors. The bioavailability of these drugs candidates has been determined by ADMET screening.

## 2. Results and discussions

### 2.1. Synthesis

The aim of this work is preparing novel acridone derivatives bearing isoxazoline moieties. The novel isoxazoline derivatives obtained from acridone (**2a–l**) were synthesized through a two-step method (Scheme 1).

The first step was the preparation of the dipolarophile by N-allytion of acridone using solid–liquid phase transfer catalyst. Stirring acridone with allyl bromide in the presence of tetra-n-butylammonium bromide (TBAB) as catalyst and anhydrous potassium carbonate in DMF at 80 °C give compound **1a-b** with good yields.

The 3,5-disubstituted isoxazolines were obtained by 1,3-dipolar cycloaddition reaction between an appropriately substituted nitrile oxides and N-allyl acridones. At the outset, our investigation focused on exploring the 1,3-dipolar cycloaddition reaction conditions between benzaldoxime and the dipolarophiles **1a**. For that, we adopted in the first step a conventional protocol based on the generation "*in situ*" of nitrile oxide in the presence of sodium hypochlorite (NaOCl) at 0 °C in the biphasic mixture $H_2O/CH_2Cl_2$ (Table 1). The reaction resulted in the formation of the desired 3,5-disubstituted isoxazoline **2a** but with very low yield ranging from 10 to 12%. This result could be explained by the low solubility of dipolarophile **1a** in water. In order to increase the yield of the 1,3-dipolar cycloaddition reaction, we turned our attention to the development of a process for the synthesis of isoxazoline derivatives based on the generation of nitrile oxide "*in situ*" from N-hydroxybenzimidoyl chloride as well as adopting a microwave assisted synthesis method. As shown in Table 1, different reaction conditions were probed to improve the yield of compound **2a**.

The results indicated in Table 1 show that the use of alkyne **1a** (1 mol equiv) and N-hydroxybenzimidoyl chloride (1.2 mol equiv) in the presence of triethylamine at 50 °C in chloroform afforded 3,5-disubstituted isoxazoline **2a** in good yield (75%). Moreover, strong acceleration of the cycloaddition reaction under microwave irradiation was noticed in comparison to conventional conditions that required 6–24 h of agitation against 20–25 min under microwave irradiation.

With the optimized reaction conditions in hand (Table 1, entry 4 and 6), we synthesized novel isoxazoline derivatives **2a-l** (Scheme 1, Table 2) by changing the starting substrates. With the different *para*- or *meta*-substituted N-hydroxybenzimidoyl chlorides used in this work, the regioselectivity of the reaction was established since no 3,4-disubstituted isoxazole regioisomers were observed. Moreover, electron donating as well as electron withdrawing N-hydroxybenzimidoyl chlorides gave similar results, except in the case of compounds **2e** and **2f** we obtained mediocre yields. The compounds (**2a-l**) were purified by column chromatography and/or recrystallization method. Purified compounds were characterized using IR, NMR and Mass spectrometry.

The IR spectra of novel isoxazoline derivatives obtained from acridone (**2a-l**) showed characteristic absorption bands in the region of 1640–1635 $cm^{-1}$ corresponding to the vibration of the carbonyl of acridone ring (C═O) and imine group of isoxazoline nucleus showed the C═N stretching frequency at 1605–1600 $cm^{-1}$. The $^1H$ NMR spectra of compounds (**2a-l**) showed aromatic protons between 8.63 and 6.67 ppm. We also noticed the presence of two signals as double doublet between 4.78 and 4.55 ppm attributable to the two protons of the methylene group (N─$CH_2$), as well as two double doublet between 3.56 and 3.27 ppm related to the methylene protons ($CH_2$) of isoxazoline ring, in addition to a multiplet between 5.40 and 5.30 ppm assigned to the proton (C─H) of isoxazoline nucleus. The chemical displacements of the proton (CH) of isoxazoline nucleus are in the order of 5.4 ppm, whereas in the case of 3,4-disubstituted isoxazoline is expected to be higher values due to the oxygen-attracting effect. These results confirm the regioselectivity of the cycloaddition reaction. $^{13}C$ NMR spectra of compounds (**2a-l**) confirm the formation of 3,5-disubstituted isoxazoline. The chemical displacements observed for the CH carbon of the isoxazoline nucleus between 79 and 78 ppm find their explanation in the oxygen attractor effect of the isoxazolic nucleus. In addition the signals between 50 and 48 ppm and 38 ppm corresponding to the CH2 groups, as well as a signal between 157 and 156 ppm relative to the carbon C═N of the isoxazoline ring and another signal between

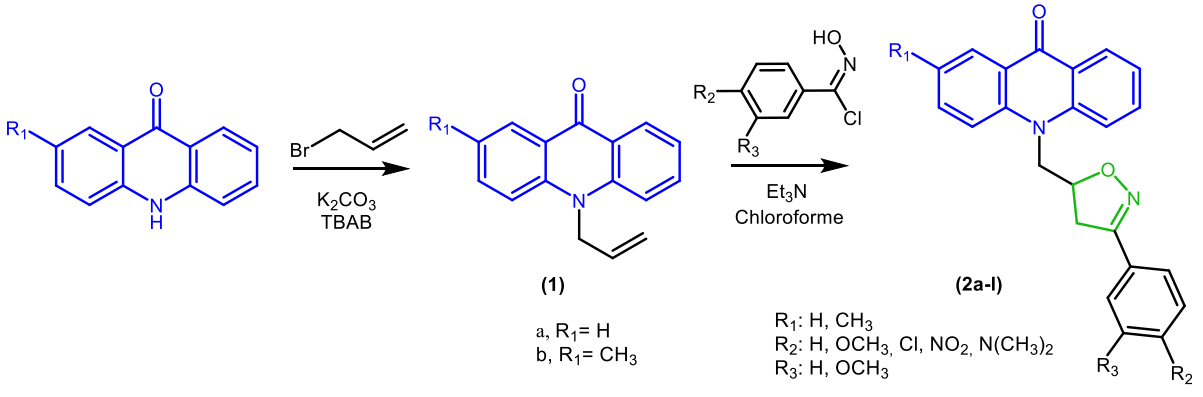


**Scheme 1** Synthesis route of novel isoxazoline derivatives from acridone (**2a-l**).

**Table 1** Optimization of the reaction conditions.[a]

| Entry | *Base* | Solvent | Temp. (°C) | *Time* | *Yield%* |
|---|---|---|---|---|---|
| 1[b] | *NaOCl* | $CH_2Cl_2/H_2O$ | 0–5 °C | 24 h | 14 |
| 2 | $Et_3N$ | $CH_2Cl_2$ | *RT* | 24 h | 60 |
| 3 | $Et_3N$ | $CHCl_3$ | *RT* | 24 h | 68 |
| 4 | $Et_3N$ | $CHCl_3$ | 50 °C | 8 h | 75 |
| 5 | $Et_3N$ | *Toluene* | 50 °C | 6 h | 60 |
| 6[c] | $Et_3N$ | $CHCl_3$ | 50 °C | 25 min | 89 |
| 7[c] | $Et_3N$ | *Toluene* | 70 °C | 20 min | 80 |

[a] Reaction conditions: **1a** (1 mmol), N-hydroxybenzimidoyl chloride (1.2 mmol), TEA (1.2 mmol), solvent (5 mL).
[b] Reaction conditions: **1a** (1 mmol), benzaldoxime (1.2 mmol), 13% aq NaOCl (2 mmol), solvent (5 mL).
[c] Reaction conditions: **1a** (1 mmol), N-hydroxybenzimidoyl chloride (1.2 mmol), TEA (1.2 mmol), solvent (5 mL) MW 200 W max.

**Table 2** Synthesized compounds **2a-l.**

| *Compounds* | *R1* | *R2* | *R3* | *Yield%* [a] | *Yield%* [b] |
|---|---|---|---|---|---|
| 2a | *H* | *H* | *H* | 70 | 86 |
| 2b | – | *OMe* | H | 79 | 89 |
| 2c | – | *Cl* | H | 63 | 68 |
| 2d | – | $NO_2$ | H | 71 | 80 |
| 2e | – | $N(CH_3)_2$ | H | 60 | 66 |
| 2f | | *OH* | OMe | 65 | 66 |
| 2g | $CH_3$ | *H* | *H* | 76 | 81 |
| 2h | – | *OMe* | H | 70 | 84 |
| 2i | – | *Cl* | H | 68 | 67 |
| 2j | – | $NO_2$ | H | 72 | 80 |
| 2k | – | $N(CH_3)_2$ | H | 63 | 64 |
| 2l | | *OH* | OMe | 60 | 65 |

[a] Reaction conditions: dipolarophile (1 mmol), dipole (1.2 mmol), TEA (1.2 mmol), chloroform (5 mL) at 50 °C.
[b] Reaction conditions: Reaction carried out under microwave irradiation (20–25 min).

178 and 176 ppm attributed to the carbonyl (C═O) of the acridone nucleus.

### 2.2. Antibacterial activity

The novel acridones **2a-l** have been studied to evaluate their antibacterial activity against Gram (−) bacteria (*E. coli, P. putida and K. pneumoniae)* and Gram (+) bacteria (*S. aureus*). The antibacterial activities have been primarily tested by agar diffusion method. Then, minimum inhibitory concentrations (MIC) were determined for the synthesized compounds. Chloramphenicol was used as positive control for antibacterial activities. Results are displayed in Table 3 as minimum inhibitory concentrations (MIC) in µg/mL. The antibacterial activity results indicate that the tested compounds displayed various degrees of inhibition against the four tested bacteria species. The highest antibacterial activity was obtained against *S. aureus* strains. Compound **2k** with methyl on acridone ring and N, N-dimethylamine on the phenyl group showed the best antibacterial activity against *P. putida* with MIC value 38.57 µg/mL, which is very close to the known commercial antibiotic chloramphenicol with MIC value 37.03 µg/mL. While compound **2a** with phenyl and hydrogen at C-2 on the acridone ring on the isoxazoline-acridone moiety, showed good activity against *E. coli* strains with MIC value 26.95 µg/mL, compared to the standard drug Chloramphenicol with MIC value 22.41 µg/mL. In addition, the compound **2 h** with *p*-methoxy on the phenyl group and methyl at C-2 on the acridone ring exhibited high potential of antibacterial activity against *S. aureus* with MIC = 24.60 µg/mL. The antibacterial activity against the tested Gram-positive and Gram-negative pathogens indicate that the replacement of the allyl group with isoxazoline nucleus enhanced the antibacterial potential against Gram-negative bacteria and Gram-positive bacteria for compounds **2a-l**, whereas no significant differences of the antibacterial activity between the N-allyl acridones and acridones against all bacteria were noticed. The antibacterial activity for the isoxazoline-acridone derivatives was increased significantly, especially for *P. putida* when the 2-methylacridone-isoxazoline skeleton was substituted by N,N-dimethylamine on the phenyl group.

### 2.3. In silico ADMET prediction and evaluation of lipinski's 'Rule of 5'

*In silico* ADMET analysis was performed to evaluate the drug-likeness and pharmacokinetic properties of the synthesized compounds **2a-l**. On this purpose, pkCSM online tool

**Table 3** MIC values (μg/mL) of the tested compounds against *E. coli, P. putida, K. pneumoniae* and *S. aureus* strains.

| *Compounds* | *Staphylococcus aureus* | *Escherichia coli* | *Klebsiella pneumoniae* | *Pseudomonas putida* |
|---|---|---|---|---|
| Acridone | *122.83* | *133.41* | *137.93* | *156.31* |
| 2-methylacridone | *118.43* | *124.22* | *130.43* | *145.52* |
| 1a | *97.10* | *80.66* | *97.25* | *100.95* |
| 1b | *83.20* | *70.14* | *102.20* | *115.20* |
| 2a | *39.57* | *26.95* | *71.00* | *88.48* |
| 2b | *32.15* | *36.88* | *65.00* | *74.64* |
| 2c | *32.15* | *42.15* | *74.64* | *91.00* |
| 2d | *35.26* | *32.75* | *74.64* | *61.00* |
| 2e | *41.78* | *49.57* | *65.00* | *74.64* |
| 2f | *39.12* | *50.12* | *60.10* | *83.44* |
| 2g | *34.78* | *43.23* | *71.00* | *81.27* |
| 2h | *24.60* | *34.39* | *65.00* | *56.55* |
| 2i | *28.39* | *30.39* | *74.64* | *61.00* |
| 2j | *30.12-* | *50.12* | *80.10* | *56.55* |
| 2k | *33.74* | *35.88* | *65.00* | *38.57* |
| *2 l* | *30.12* | *30.39* | *76.23* | *56.55* |
| Chloramphenicol | *11.65* | *22.41* | *15.38* | *37.03* |
| DMSO | – | – | – | – |

(Pires et al., 2015) and DruLito software ("Drug Likeness Tool (DruLiTo 1)," n.d.) were used. Therefore, human intestinal absorption, blood–brain barrier penetration (BBB), acute oral toxicity, skin sensitization, AMES toxicity, HEGR inhibitor and some druglike properties were calculated.

Based on Lipinski rules of 5 compounds with molecular mass less than 500 Da, 5 hydrogen bond donors, 10 hydrogen bond acceptors, and with an octanol–water partition coefficient log P less than 5 are likely absorbed. Table 4 shows that the studied compounds (**2a-2 l**) have high lipophilicity property (LogP = 3.05–3.86), molecular weight MW (354.14–414.16), H-bond acceptor (< 10) and H-bond donor (< 5) and total polar surface area (≤140) which confirmed the desirable drug likeness criteria of these synthetized drugs candidates. Drugs with poor bioavailability are considered as inefficient because major portion of a dose never reaches the plasma to exert the pharmacological effect. In general, the predictive model of pKCSM indicates that molecules with predicted values > 0.9 have high Caco2- permeability, human intestinal absorption values less than 30% are poorly absorbed, low values of total clearance means high half-life and molecules with logBB < −1 are poorly distributed to the brain (Ghaleb et al., 2019).

The predicted bioavailability of the synthetized compounds **2b** and **2h** presented in Table 5 shows an excellent pharmacokinetics property, they present high Caco2-permeability (1.08–1.06) and intestinal absorption (98.64–99.19), they are poorly distributed to the brain (−0.04; −0.06) with total clearance (0.31–0.35). The subtype of cytochrome P450 CYP2D6 indicates that they could not be a substrates or inhibitors of this main subtype, which can decrease the chance of drug-drug interactions. They present no hERG inhibitory, hepatotoxicity or skin sensibilization, while compounds (**2d**, **2f**, **2j**, **2l**) show low Caco2- permeability and the compounds (**2a**, **2c**, **2e**, **2g**, **2i**, **2k**) can exhibit blood barrier permeability. Moreover, the

**Table 4** Lipinski's properties of the newly synthesized compounds **2a-l.**

| Compound | Property | | | | | | Lipinski violation |
|---|---|---|---|---|---|---|---|
| | Log*P* | H-bond acceptor | H-bond donor | Polar surface area ($A^2$) | Rotatable Bonds | Molecular weight | |
| **2a** | *3.47* | *2* | *0* | *41.9* | *3* | *354.14* | *0* |
| **2b** | *3.08* | *3* | *0* | *51.13* | *4* | *384.15* | *0* |
| **2c** | *3.41* | *2* | *0* | *41.9* | *3* | *388.1* | *0* |
| **2d** | *3.05* | *2* | *0* | *85.04* | *4* | *399.12* | *0* |
| **2e** | *3.37* | *3* | *0* | *45.14* | *4* | *397.18* | *0* |
| **2f** | *3.0* | *4* | *1* | *71.36* | *4* | *400.14* | *0* |
| **2g** | *3.86* | *2* | *0* | *41.9* | *3* | *368.15* | *0* |
| **2h** | *3.47* | *3* | *0* | *51.13* | *4* | *398.16* | *0* |
| **2i** | *3.81* | *2* | *0* | *41.9* | *3* | *402.11* | *0* |
| **2j** | *3.45* | *2* | *0* | *85.04* | *4* | *413.14* | *0* |
| **2k** | *3.76* | *3* | *0* | *45.14* | *4* | *411.19* | *0* |
| **2l** | *3.39* | *4* | *1* | *71.36* | *4* | *414.16* | *0* |

**Table 5** *In silico* ADMET prediction of synthesized compounds **2a-l.**

| Name | Absorption | | Distribution | Metabolism | | | | | | Excretion | Toxicity | | | | |
|---|---|---|---|---|---|---|---|---|---|---|---|---|---|---|---|
| | Caco2 permeability | Intestinal absorption (human) | Blood brain barrier Permeability | CYP | | | | | | Total Clearance | hERG inhibitor | Max. tolerated dose (human) | Hepatot-oxicity | Skin Sensitization | AMES |
| | | | | 2D6 substrate | 3A4 substrate | 1A2 inhibitor | 2C19 inhibitor | 2C9 inhibitor | 2D6 inhibitor | 3A4 inhibitor | | | | | |
| | (log mol/L) | Numeric (% Absorbed) | (logBB) | Categorical (Yes/No) | | | | | | Numeric log (ml/min/kg) | (Yes/No) | log(mg/kg/Day) | log (LC50) | (Yes/No) | (Yes/No) |
| 2a | 1.06 | 97.51 | 0.27 | No | Yes | Yes | Yes | Yes | No | Yes | 0.31 | No | 0.40 | No | No | No |
| 2b | 1.08 | 98.64 | −0.04 | No | Yes | Yes | Yes | Yes | No | Yes | 0.33 | No | 0.34 | No | No | Yes |
| 2c | 1.05 | 96.10 | 0.24 | No | Yes | Yes | Yes | Yes | No | Yes | 0.15 | No | 0.30 | No | No | Yes |
| 2d | 0.42 | 95.74 | −0.69 | No | Yes | Yes | Yes | Yes | No | Yes | 0.33 | No | 0.14 | No | No | No |
| 2e | 1.05 | 98.85 | 0.19 | No | Yes | Yes | Yes | Yes | No | Yes | 0.51 | No | 0.29 | No | No | No |
| 2f | 0.58 | 96.06 | −0.49 | No | Yes | Yes | Yes | Yes | No | Yes | 0.34 | No | 0.18 | No | No | No |
| 2g | 1.05 | 98.05 | 0.27 | No | Yes | Yes | Yes | Yes | No | Yes | 0.34 | No | 0.3 | No | No | Yes |
| 2h | 1.05 | 99.19 | −0.06 | No | Yes | Yes | Yes | Yes | No | Yes | 0.35 | No | 0.24 | No | No | No |
| 2i | 1.04 | 96.65 | 0.24 | No | Yes | Yes | Yes | Yes | No | Yes | 0.11 | No | 0.19 | No | No | No |
| 2j | 0.49 | 96.29 | −0.69 | No | Yes | Yes | Yes | Yes | No | Yes | 0.35 | No | 0.01 | No | No | No |
| 2k | 1.04 | 99.40 | 0.19 | No | Yes | Yes | Yes | Yes | No | Yes | 0.53 | No | 0.18 | No | No | No |
| 2l | 0.66 | 96.61 | −0.50 | No | Yes | Yes | Yes | Yes | No | Yes | 0.36 | No | 0.10 | No | No | No |

drug candidate **2b** shows an AMES toxicity which can be a mutagenic compound and therefore acts as a carcinogen. While the synthetized compound **2h** present good pharmacokinetics properties (absorption, distribution, metabolism, excretion and toxicity). In general, most synthetized compounds can be considered as promising drugs candidates for further studies.

### *2.4. Molecular docking studies*

Molecular docking was used to understand the binding modes and to support the antibacterial activity of the synthesized compounds obtained experimentally, also to elucidate new information for further structural optimization.

The transcriptional regulator (TtgR) enzyme of *P. putida* is a HTH-type transcriptional repressor that controls expression of the TtgABC efflux pump, which is the main contributor to resistance against several antimicrobials agents (Terán et al., 2003). Moreover, previous studies on the TtgR multidrug binding potential have shown that it binds with moderate to high affinity to plant-derived compounds such as phloretin and naringenin (Alguel et al., 2007b; Choudhury, 2010). Concerning *E. coli,* MenB or dihydroxynaphthoic acid synthetase is interesting enzyme in the biosynthesis of menaquinone. The enzymes in the biosynthetic pathway of bacterial menaquinone are potential targets for novel antibacterial drug (Sharma et al., 1992). In this work, the molecular docking studies of the synthesized compounds have been applied to determine the different type of interactions and clarify the probable binding modes between acridone derivatives and transcriptional regulator (TtgR) enzyme (PDB ID : 2UXI) of *P. putida* (Alguel et al., 2007a) and *E. coli* MenB, OSB-NCoA complex (PDB ID : 3 T88) respectively (Li et al., 2011).

The molecular docking setup was first validated by performing self-docking of the co-crystalized ligands (Phloretin) and (S0N) in the active site of transcriptional regulator (TtgR) enzyme (PDB ID : 2UXI) of *P. putida* and *E. coli* MenB, OSB-NCoA (PDB ID : 3T88), respectively. The results of self-docking validation show small RMSD between the docked pose and the experimental co-crystallized inhibitor pose with 0.70 Å for (transcriptional regulator (TtgR) enzyme) and 1.52 Å for (*E. coli* MenB, OSB-NCoA), which is satisfactory (less than 2 Å). In addition, all the twelve acridones were docked into the binding pocket of transcriptional regulator (TtgR) enzyme and *E. coli* MenB, OSB-NCoA successfully.

The analysis of the active site of transcriptional regulator (TtgR) enzyme, reveals that all the synthesized compounds **2a-l** are making various close contacts with the residues lining the active site of transcriptional regulator (TtgR) enzyme, the interacting amino acids of all compounds are shown at Table 6. The analysis of best scoring pose of compound (**2k)** (stable conformation) in the transcriptional regulator (TtgR) enzyme pocket of 2XUT showed significant hydrogen bonding as well as hydrophobic interactions between them (Fig. 2). The isoxazoline ring and phenyl group exhibits hydrophobic interactions with the residues *His70*, *Val96*, *Ala74, Leu66, Leu92* and *Leu100*. Carbonyl group of acridone nucleus exhibited hydrogen bonding interactions with *Asn110*. The high docking scores of compounds of **2k**, **2j**, **2h** and **2l** reveal that these compounds are well accommodated in the active site of enzyme and they strongly interact within the active site of transcrip-

**Table 6** The interactions and binding affinities of the synthesized compounds **2a-l.**

| | *2XUI* | | *3T88* | |
|---|---|---|---|---|
| | Interacting residues | Binding affinity | Interacting residues | Binding affinity |
| 2a | *His67, Met89, Val96, His70, Leu66, Leu92, Val171, Cys137, Ile141, Ala74* | −7.03 | ***Thr155, Gly133***, *Val159, Tyr97, Gly132* | −7.04 |
| 2b | ***Asn110***, *His70, Met89, His67, Val96, Leu92, Val171, Cys137, Ile141, Ala74* | −7.58 | *Val159, Gly133, Gly85, Tyr97, Val108* | −6.74 |
| 2c | *His70, Met89, His67, Val96, Leu100, Ile175, Leu66, Leu92, Val171, Cys137, Ile141, Ala74* | −7.27 | *Val159, Gly164, Asp163, Phe162, Gly133* | −6.53 |
| 2d | ***Asn110***, *His70, Met89, His67, Val96, Leu66, Leu92, Val171, Cys137, Ile141, Ala74* | −7.71 | ***Thr155***, *Gly132, Gly164, Phe162* | −6.96 |
| 2e | ***Asn110***, *His70, His67, Val96, Leu66, Leu92, Cys137, Ala74, Ser77, Glu78, Gly140, Phe168, Val134* | −7.91 | *Phe162, Gly133, Ser84* | −6.96 |
| 2f | *Val134, Cys137, Phe168, His70, Val96, Leu92* | −7.34 | *Asp163, Phe162, Gly164, Gly133* | −7.01 |
| 2g | *His70, His67, Val96, Leu66, Leu92, Cys137, Ala74, Phe168, Met89, Ala144, Val171, Ile141* | −7.43 | *Phe162, Asp163, Gly164, Gly133* | −6.69 |
| 2h | ***Asn110***, *Met89, His70, His67, Val96, Leu92, Cys137, Ala74, Phe168, Ile141, Ala144, Val171* | −8.01 | *Phe162, Ser84, Gly164, Gly133, Gly86* | −7.03 |
| 2i | *Met89, Phe168, His70, His67, Val96, Leu92, Cys137, Ala74, Ile141, Ala144, Val171, Ile175, Leu100* | −7.68 | ***Thr155,*** *Val159, Gly132, Ile131, Ala47, Val44, Lys89, Ser84* | −6.80 |
| 2j | ***Asn110***, *Met89, Phe168, His70, His67, Val96, Cys137, Ala74, Ile141, Ala144, Val171, Leu66, Leu92* | −8.14 | *Phe162, Asp163, Gly164, Gly133* | −6.92 |
| 2k | *Asn110, Phe168, His70, His67, Val96, Cys137, Ala74, Ser77, Leu66, Leu92, Glu78, Leu100, Val134, Gly140* | −8.33 | ***Thr155***, *Gly133, Gly132, Ile131, Val159, Ala47, Lys89, Val44,Arg45* | −7.01 |
| 2l | ***Asn110***, *Phe168, His67, Val96, Cys137, Ala74, Leu66, Leu92, Leu100, Val134, Ile141* | −7.84 | ***Thr155***, *Val108, Leu106* | −7.04 |

In Bold: H-bonding interaction.

tional regulator (TtgR) enzyme. Relying on the different interactions of the synthesized compounds presented in Fig. 2, Table 6, it can be concluded that the most active compounds have H-bond interaction with *Asn110* and hydrophobic interactions with the receptor indicating the crucial role that play to inhibit the transcriptional regulator (TtgR) enzyme, this results has been demonstrated by previous researches (Choudhury, 2010; Paul and Choudhury, 2010; Zhang et al., 2017).

Concerning *E. coli* MenB, OSB-NCoA, the stable pose of the most active compound **2a** showed two favorable hydrogen bonds between the nitrogen and oxygen atoms of isoxazoline nucleus and the hydrogen of the side chain of *Thr155* and *Gly133*, respectively. The phenyl and acridone core shows hydrophobic interactions with *Val115* and *Gly132* (Fig. 3). Also compounds **2d**, **2i** and **2l** showed one favorable hydrogen bond between the nitro group of isoxazoline ring and the hydrogen of the side chain of *Thr155*, besides hydrophobic interactions. The molecular docking results of the different interactions of the synthesized compounds presented in Table 6, indicate that the most active compounds **2a, 2i, 2d** and **2l** have H-bond interaction with the hydrogen of the side chain of *Thr155* in the active site of *E. coli* MenB, OSB-NCoA. Moreover, all synthesized compounds **2a-l** bind to the active site of *E. coli* MenB, OSB-NCoA and share largely homogeneous in binding mode specially with *Val159, Gly133, Phe162 and Asp163* to several *E. coli* MenB inhibitors reported in the literature (Fahim and Farag, 2020; Mahmoud et al., 2017). The high docking scores of compounds of **2a, 2i, 2d** and **2l** reveal that these compounds are well accommodated in the active site of enzyme and they strongly interact within the active site of *E. coli* MenB, OSB-NCoA. In consequence, molecular docking studies showed strong binding affinity of **2a** into the active site of *E. coli* MenB, OSB-NCoA, which could be responsible for its significant *in vitro* antibacterial activity especially against *E. coli*.

The molecular docking results presented in the Fig. 2 shows the interactions of most promising derivatives 2k and 2h with TtgR enzyme, the compound **2k** is stabilized into the receptor pocket with hydrogen bond, pi-alkyl and Van der-waals interactions. The compound **2h** shows hydrogen bond, pi-sulfur and different pi-alkyl interactions, while the co-crystalized compound shows Van der-waals and pi-alkyl interactions. The Fig. 3 presents the different interactions of the most promising compounds (**2a** and **2h**) and the co-crystalized compound (o-succinylbenzoyl-N-coenzyme A) with *E. coli* MenB, OSB-NCoA complex. The compound 2a is stabilized with two hydrogen bonds, pi-alkyl and Van der-waals interactions, and the compound 2 h shows pi-ion with different Van der-waals interactions, while the co-crystalized compound is stabilized with four hydrogen bonds, pi-cation and pi-alkyl interactions.

## 3. Conclusion

The synthesis of novel acridone-isoxazoline derivatives **2a-l** has been accomplished with a very accessible way under mild conditions through the 1,3-dipolar cycloaddition of various aryl nitrile oxides *in situ* generated and N-allyl acridones. The molecular structures of the obtained compounds are supported by $^{1}$H NMR, $^{13}$C- NMR, IR and MS spectra. All the synthesized compounds were evaluated for their antibacterial activ-

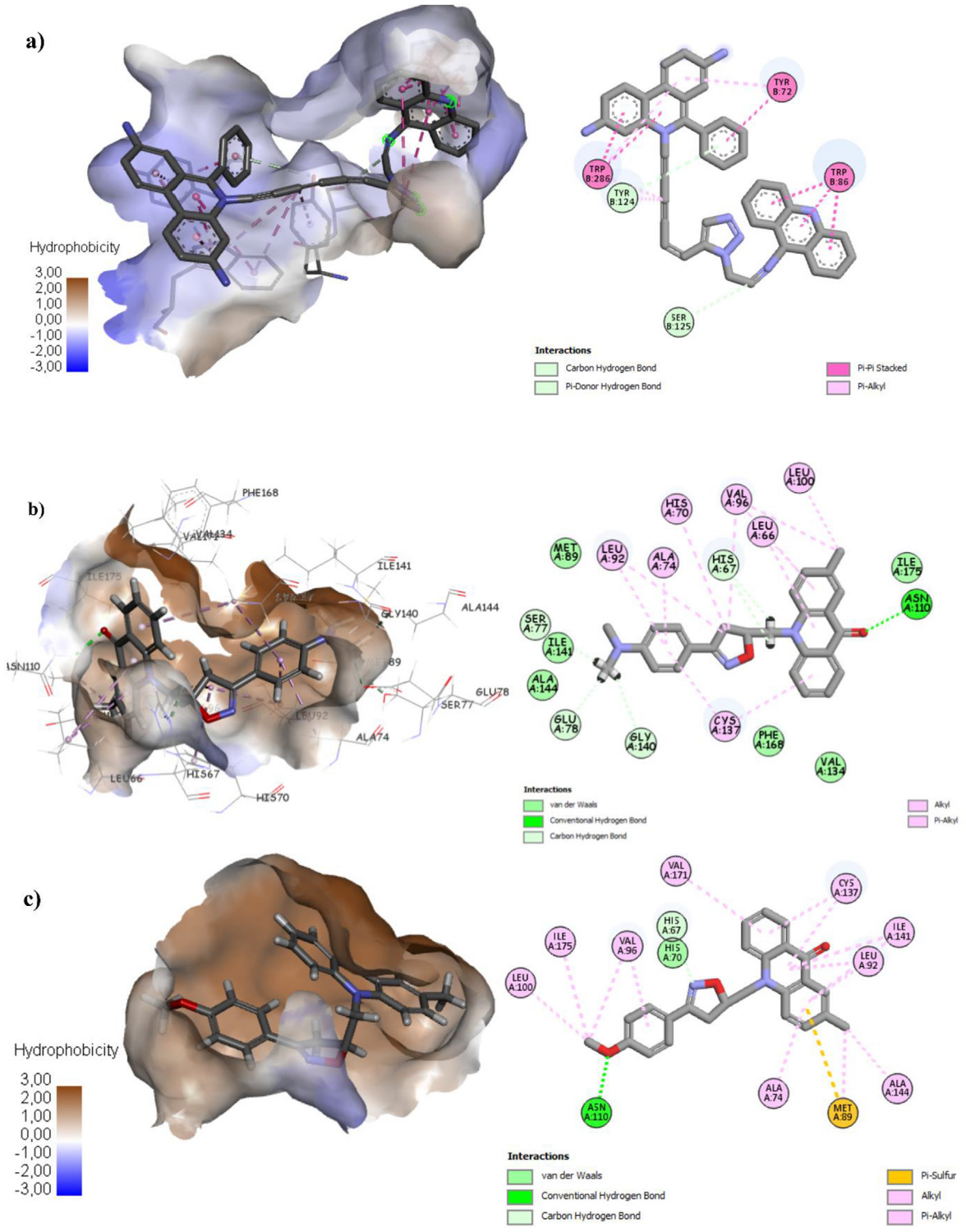


**Fig. 2** (a) Binding mode of co-crystalized compound with TtgR enzyme. (b) Binding mode of compound most active compound **2k** with TtgR enzyme. (c) Binding mode of compound **2h** with TtgR enzyme.

ity, compounds **2a** and **2k** were found to be the most potent agents against *E. coli* and *P. putida,* respectively. To determine the stable conformation of the synthetized compounds into the receptor pocket and understand receptor-ligands interactions molecular docking was applied. The docking results suggest that compounds **2l**, **2h**, **2k** and **2a** are the most potent inhibitor of transcriptional regulator (TtgR) enzyme of *P. putida* and *E. coli* MenB, OSB-NCoA, respectively. Moreover, *in silico* ADMET screening results showed that the synthesized compounds are easily absorbed and present a good bioavailability.

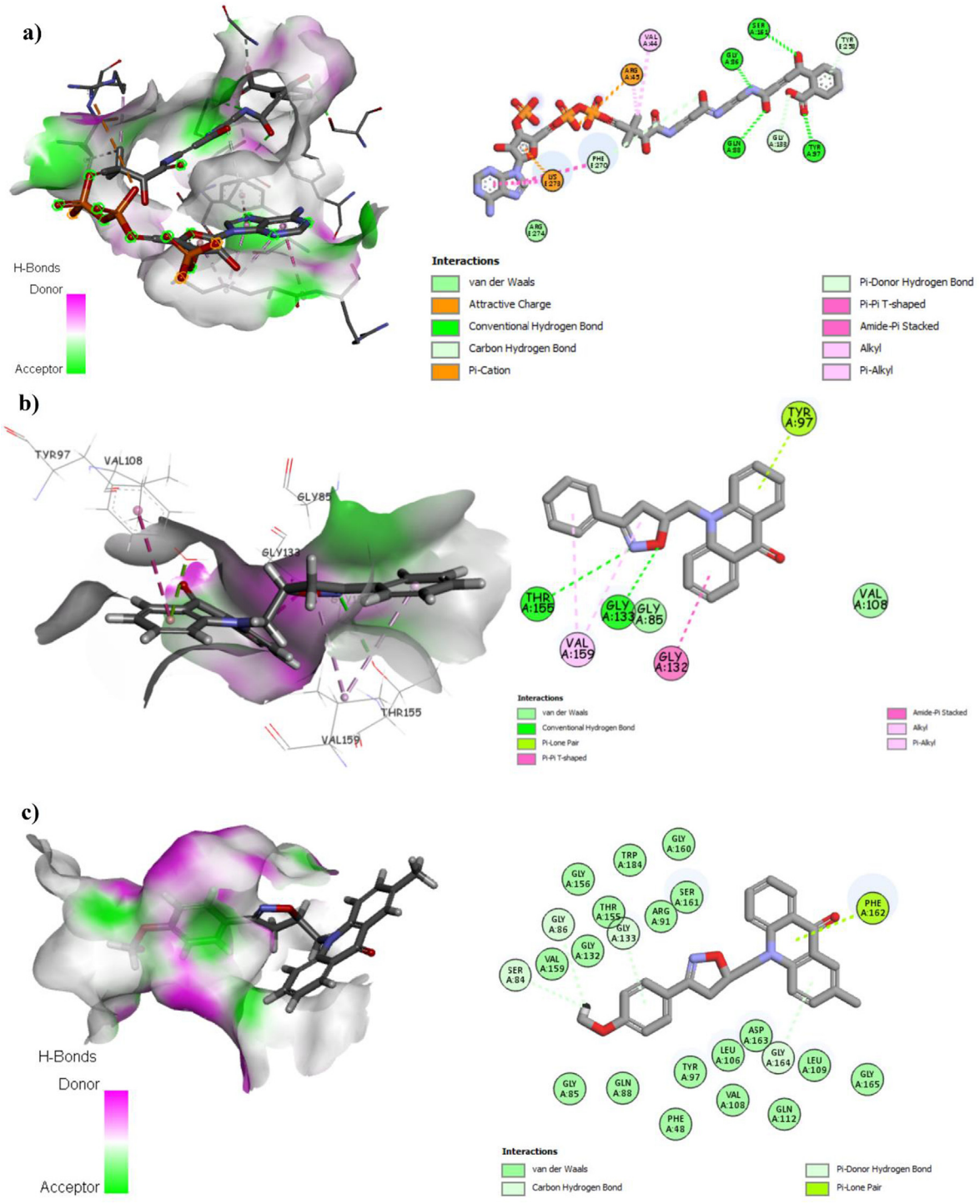


**Fig. 3** (a) Binding mode of the co-crystalized ligand with *E. coli* MenB, OSB-NCoA complex, the hydrogen bonds are presented in green dashed lines. (b) Binding mode of compound **2a** with *E. coli* MenB, OSB-NCoA complex, the hydrogen bonds are presented in green dashed lines. (c) Binding mode of compound **2h** with *Escherichia coli* MenB, OSB-NCoA complex.

## 4. Experimental

### 4.1. Materials

All materials were purchased from commercial suppliers. IR spectra were recorded using JASCO FT-IR 4100 spectrophotometer. The $^{1}H$, $^{13}C$ NMR spectra was recorded with Bruker Avance 300. Mass spectrometric measurements were recorded using Exactive™ Plus Orbitrap Mass Spectrometer. Microwave irradiation was carried out with CEM Discover™.

### 4.2. Antibacterial activity

The synthesized compounds (**2a-l**) were tested for their *in vitro* antibacterial activity against Gram (−) bacteria (*E. coli, P. putida and K. pneumoniae)* and Gram (+) bacteria (*S. aureus*). The antibacterial activities have been primarily tested by agar diffusion method, the active compounds were subjected to the determination of the MIC, using the broth microdilution method. The microorganisms used in this study are pathogenic germs isolated from urine samples, collected from patients suspected of urinary tract infection (UTI), provided by Mohammed V Hospital in Meknes. Bacterial inoculums were prepared by subculturing microorganisms into Mueller Hinton broth (MHB) at 37 °C for 18 h and were diluted to approximately $10^{6}$ CFU $mL^{-1}$. Initial solution with concentration 0.5 mg/mL of the compounds (**2a-l**) were prepared in DMSO, further serial dilutions were made in the microplates and 100 µL of MHB containing each test microorganism were added to the microplate (Smith et al., 2018), then incubated at 36 °C for 24 h. After incubation, 20 µL of TTC (0.04 mg/mL) were added to each microplate. The color changes of TTC from colorless to red were accepted as microbial growth (Veiga et al., 2019).

### 4.3. Docking studies

#### 4.3.1. Preparation of protein and ligands

The Discovery Studio (version 4.5) installed on windows 7 workstations was used to prepare the protein. The crystal structure of *E. coli* MenB, OSB-NCoA complex (PDB ID :3T88) (Li et al., 2011) and transcriptional regulator (TtgR) enzyme (PDB Code: 2UXI) (Alguel et al., 2007a) were retrieved from the protein data bank (PDB), [https://www.rcsb.org/]. The protein and co-crystallized ligand were isolated from the complex. The protein extracted from the complex was treated by removing all of the substructures, removing all of the water molecules and adding hydrogen atoms. The three-dimensional (3D) structures of ligands were drawn by using the chemical modeling software Avogadro (Hanwell et al., 2012). Geometry optimization tool embedded in Avogadro was used for structural refinement.

#### 4.3.2. Molecular docking

Molecular docking process between ligands and the receptor was carried out by using the AutoDock software (Morris et al., 1998). In this study, AutoDockTools, Autogrid 4.2 and Autodock 4.2 were used to prepare input files, calculate grid maps and docking simulations. Grid-point spacing of 0.375 Å and grid box of 50 × 50 × 50 Å (x, y, and z) points with the xyz-coordinated 42.921, 42.976, and 8.801 was used. After merging all non-polar hydrogen, Kollman charged were added to the receptor. All other values were set as defaults and Lamarckian genetic algorithm (GLA) search for 100 run job were used (Shirgahi Talari et al., 2015). Discovery Studio visualizer version 4.5 was used for visualization. Docking setup was first validated by self-docking of the co-crystallized inhibitor in the enzyme active. The validated molecular docking setup was then used to investigate the ligand-target interactions of the newly synthesized compounds in *E. coli* MenB, OSB-NCoA complex and transcriptional regulator (TtgR) enzyme to predict their binding pattern and to investigate their ability to satisfy the required structural features for binding interactions.

#### 4.3.3. Lipinski rule of 5 and in silico ADMET prediction:

Computational approaches have improved the success rate of drug development and reduced the experimental trials. In this concept an *in silico* ADMET and drug likeness studies were applied to the synthetizes compounds, using pkCSM online tool (Pires et al., 2015) and DruLito software ("Drug Likeness Tool (DruLiTo 1)," n.d.). The drug likeness was determined by predicting Log P, H-bond donor and acceptor, molecular weight. The drugs bioavailability is determining different descriptors such as Caco2- permeability, human intestinal absorption, blood brain barrier permeability, subtypes of cytochrome P450, total clearance and AMES toxicity.

#### 4.3.4. Synthesis of acridon-isoxazoline derivatives (2a-l)

To a solution of N-allyl acridone **1** (1.2 g, 5 mmol) in chloroform (15 mL), N-hydroxybenzimidoyl chloride (1 g, 6.4 mmol) and TEA (0.64 g, 6.4 mmol) were added at room temperature, the reaction mixture was stirred at 50 °C for 6 h. Then, water (40 mL) was added and the mixture was extracted with chloroform, the organic layer was evaporated in high vacuum, and the obtained product was purified by recrystallization in DMF or by flash chromatography on silica gel using hexane/diethyl ether (2:5).

*4.3.4.1. 10-((3-phenyl-4,5-dihydroisoxazol-5-yl)methyl)acridin-9(10H)-one (**2a**).* Yellow solid; yield: 86%, mp = 185 °C**.** IR (KBr): 3012, 2975, 1640, 1600, 1596 $cm^{-1}$. $^{1}H$ NMR (300 MHz, DMSO $d_6$, 25 °C, TMS): 8.40 (d, $J$ = 8.1 Hz, 2H, H1,H8), 8.09–7.66 (m, 6H), 7.65–7.45 (m, 3H), 7.39 (t, $J$ = 7.5 Hz, 2H), 5.28–5.20 (m, 1H), 5.03 (dd, $J$ = 17.0, 9.2 Hz, 1H), 4.72 (dd, $J$ = 17.0, 8.1 Hz, 1H), 3.42 (dd, $J$ = 16.7, 7.1 Hz, 1H), 3.13 (dd, $J$ = 16.7, 7.1 Hz, 1H).. $^{13}C$ NMR (75 MHz, DMSO $d_6$, 25 °C, TMS): 177.72, 156.09, 142.01, 135.46, 134.05, 128.43, 128.08, 122.60, 121.76, 121.47, 121.30, 114.94, 114.31, 78.10, 48.47, 38.24. MS (ESI) for $C_{23}H_{18}N_2O_2$ $[M+H]^+$, calcd: 355.1441, found: 355.1440.

*4.3.4.2. 10-((3-(4-methoxyphenyl)-4,5-dihydroisoxazol-5-yl)methyl)acridin-9(10H)-one (**2b**).* White solid; yield: 89%, mp = 148 °C. IR (KBr): 3014, 2975, 1635, 1603, 1594 $cm^{-1}$. $^{1}H$ NMR (300 MHz, CDCl3, 25 °C, TMS): 8.61 (d, $J$ = 8.1 Hz, 2H, H1,H8), 7.76–7.52 (m, 8H), 7.34 (t, $J$ = 7.3 Hz, 1H), 6.96 (d, $J$ = 8.4 Hz, 1H), 5.35 (m, 1H), 4.78 (dd, $J$ = 16.1, 7.5 Hz, 1H), 4.69–4.45 (dd, $J$ = 16.1, 7.5 Hz, 1H), 3.88 (s, 3H, OCH3), 3.55 (dd, $J$ = 17.0, 9.4 Hz, 1H), 3.4 –3.07 (dd, $J$ = 17.0, 9.4 Hz, 1H). $^{13}C$ NMR

(75 MHz, CDCl3, 25 °C, TMS): 177.92, 161.49, 156.57, 142.31, 135.46, 134.05, 128.43, 128.08, 122.60, 121.76, 121.47, 121.30, 114.94, 114.31, 78.47, 55.41, 48.72, 38.72. MS (ESI) for $C_{24}H_{20}N_2O_3$ $[M+H]^+$, calcd: 385.1510, found: 385.1510.

*4.3.4.3. 10-((3-(4-chlorophenyl)-4,5-dihydroisoxazol-5-yl) methyl)acridin-9(10H)-one (**2c**)*. Yellow solid; yield: 68%, mp = 159 °C**.** IR (KBr): 3011, 2985, 1639, 1604, 1590 $cm^{-1}$. $^1H$ NMR (300 MHz, CDCl3, 25 °C, TMS): 8.59 (dd, *J* = 8.1, 1.7 Hz, 2H, H1,H8), 7.78–7.66 (m, 2H), 7.66–7.51 (m, 4H), 7.42 (d, *J* = 8.2 Hz, 2H), 7.37–7.29 (m, 2H), 5.42–5.31 (m, 1H), 4.77 (dd, *J* = 15.4, 7.6 Hz, 1H), 4.57 (dd, *J* = 16.3, 4.5 Hz, 1H), 3.64 (dd, *J* = 16.7, 7.1 Hz, 1H), 3.23 (dd, *J* = 16.7, 7.1 Hz, 1H).$^{13}C$ NMR (75 MHz, CDCl3, 25 °C, TMS): 177.86, 156.11, 142.21, 142.08, 140.29, 136.66, 135.47, 134.06, 133.89, 131.54, 129.17, 128.04, 127.29, 122.42, 121.82, 121.53, 114.84, 79.10, 48.63, 38.29. MS (ESI) for $C_{23}H_{17}ClN_2O_2$ $[M+H]^+$, calcd: 389.1019, found: 389.1018.

*4.3.4.4. 10-((3-(4-nitrophenyl)-4,5-dihydroisoxazol-5-yl) methyl)acridin-9(10H)-one (**2d**)*. White solid; yield: 80%, mp = 198 °C**.** IR (KBr): 3000, 2987, 1638, 1605, 1598 $cm^{-1}$. $^1H$ NMR (300 MHz, CDCl3, 25 °C, TMS): 8.64 (dd, *J* = 8.0, 1.7 Hz, 2H), 8.36–8.22 (m, 2H), 8.03–7.88 (m, 2H), 7.78 (td, *J* = 8.7, 7.0, 1.7 Hz, 2H), 7.56–7.35 (m, 4H), 5.52–5.41 (m, 1H), 4.77 (dd, *J* = 15.4, 7.6 Hz, 1H), 4.67 (dd, *J* = 16.3, 4.5 Hz, 1H), 3.74 (dd, *J* = 16.7, 7.1 Hz, 1H), 3.33 (dd, *J* = 16.7, 7.1 Hz, 1H). $^{13}C$ NMR (75 MHz, CDCl3, 25 °C, TMS): 177.95, 168.76, 161.17, 148.92, 141.80, 134.50, 128.32, 127.77, 124.20, 122.90, 122.35, 114.17, 8010, 49.63, 39.29. MS (ESI) for $C_{23}H_{17}N_3O_4$ $[M + H]^+$, calcd: 400,1282, found: 400,1272.

*4.3.4.5. 10-((3-(4-(dimethylamino)phenyl)-4,5-dihydroisoxazol-5-yl)methyl)acridin-9(10H)-one (**2e**)*. Yellow solid; yield: 66%, mp = 136 °C**.** IR (KBr): 3000, 2985, 1636, 1603, 1591 $cm^{-1}$. $^1H$ NMR (300 MHz, CDCl3, 25 °C, TMS): 8.61 (d, *J* = 7.9 Hz, 2H), 7.73 (dt, *J* = 9.7, 5.1 Hz, 3H), 7.58 (dq, *J* = 15.7, 9.6, 9.1 Hz, 4H), 7.40–7.31 (m, 2H), 6.72 (d, *J* = 8.5 Hz, 1H), 5.30–5.21 (m, 1H), 4.88–4.67 (d, 1H, *J* = 14.2 Hz, 1H), 4.57 (d, *J* = 14.3 Hz, 1H), 3.54 (dd, *J* = 16.6, 6.0 Hz, 1H), 3.24 (dd, *J* = 16.2, 5.8 Hz, 1H), 3.05 (s, 6H, CH3). $^{13}C$ NMR (75 MHz, CDCl3, 25 °C, TMS): 176.43, 155.86, 152.23, 142.37, 134.08, 129.32, 128.19, 128.11, 128.03, 126.02, 121.81, 121.72, 119.63, 115.06, 111.72, 77.96, 77.46, 77.03, 76.61, 48.72, 40.13, 38.89. MS (ESI) for $C_{25}H_{23}N_3O_2$, $[M + H]^+$, calcd: 398,1862, found: 398.1852.

*4.3.4.6. 10-((3-(4-hydroxy-3-methoxyphenyl)-4,5-dihydroisoxazol-5-yl)methyl)acridin-9(10H)-one (**2f**)*. Yellow solid; yield: 66%, mp = 200 °C**.** IR (KBr): 3410, 3010, 2974, 1639, 1601, 1598 $cm^{-1}$ $^1H$ NMR (300 MHz, DMSO $d_6$, 25 °C, TMS): 9.50 (s, 1H, OH), 8.41 (dd, *J* = 8.1, 1.7 Hz, 2H), 7.48–7.41 (m, 2H), 7.30 (dd, *J* = 7.9, 1.4 Hz, 2H), 7.22–7.12 (m, 3H), 6.81 (td, *J* = 7.5, 1.5 Hz, 2H), 5.37 (m, 1H), 4.79 (dd, *J* = 16.1, 7.5 Hz, 1H), 4.65–4.40 (dd, *J* = 16.1, 7.5 Hz, 1H), 3.89 (s, 3H, $OCH_3$), 3.51 (dd, *J* = 17.0, 9.4 Hz, 1H), 3.42–3.09 (dd, *J* = 17.0, 9.4 Hz, 1H).$^{13}C$ NMR (75 MHz, DMSO $d_6$, 25 °C, TMS): 178.63, 168.83, 159.04, 148.70, 147.80, 141.33, 131.82, 126.87, 123.32, 121.86, 121.76, 121.55, 116.05, 115.83, 110.50, 79.47, 56.41, 48.79, 38.82. MS (ESI) for $C_{24}H_{20}N_2O_4$ $[M + H]^+$, calcd: 401,1483, found: 401, 1480.

*4.3.4.7. 2-methyl-10-((3-phenyl-4,5-dihydroisoxazol-5-yl) methyl)acridin-9(10H)-one (**2g**)*. Yellow solid; yield: 81%, mp = 205 °C**.** IR (KBr): 3014, 2975, 1635, 1603, 1597 $cm^{-1}$. $^1H$ NMR (300 MHz, CDCl3, 25 °C, TMS): 8.60 (dd, *J* = 8.0, 1.7 Hz, 1H, H1), 8.37 (s, 1H, H8), 7.74–7.68 (m, 3H), 7.59–7.51 (m, 3H), 7.49–7.39 (m, 3H), 7.33–7.27 (m, 1H), 5.40–5.30 (m, 1H), 4.75 (dd, *J* = 16.3, 7.5 Hz, 1H), 4.55 (dd, *J* = 16.3, 4.4 Hz, 1H), 3.56 (dd, *J* = 16.7, 10.3 Hz, 1H), 3.27 (dd, *J* = 16.7, 6.9 Hz, 1H), 2.47 (s, 3H, CH3). $^{13}C$ NMR (75 MHz, CDCl3, 25 °C, TMS): 177.86, 157.02, 142.12, 140.34, 135.48, 133.88, 131.49, 130.61, 128.88, 128.81, 128.05, 127.33, 126.85, 122.43, 122.39, 121.49, 114.91, 114.80, 78.81, 48.62, 38.45, 20.54. MS (ESI) for $C_{24}H_{20}N_2O_2$ $[M + H]^+$, calcd: 369,1560, found: 369,1560.

*4.3.4.8. 10-((3-(4-methoxyphenyl)-4,5-dihydroisoxazol-5-yl) methyl)-2-methylacridin-9(10H)-one (**2h**)*. Yellow solid; yield: 84%, mp = 165 °C**.** IR (KBr): 3010, 2970, 1640, 1604, 1590 $cm^{-1}$. $^1H$ NMR (300 MHz, CDCl3, 25 °C, TMS): 8.61 (dd, *J* = 8.0, 1.5 Hz, 1H, H1), 8.38 (s, 1H, H8), 7.81–7.76 (m, 2H), 7.63–7.41 (m, 4H), 7.31 (d, *J* = 6.6 Hz, 1H), 7.12 (dd, *J* = 8.5, 6.4 Hz, 1H), 6.69 (d, *J* = 8.6 Hz, 1H), 5.33 (m, 1H), 4.71 (dd, *J* = 15.2, 6.1 Hz, 1H), 4.54 (dd, *J* = 15.3 Hz, 1H), 3.59–3.41 (m, 1H), 3.38–3.10 (m, 1H), 3.86 (s, 3H, CH3), 2.48 (s, 3H, CH3). $^{13}C$ NMR (75 MHz, CDCl3, 25 °C, TMS): 177.89, 161.41, 156.57, 142.31, 135.46, 134.05, 128.43, 128.08, 122.60, 121.76, 121.47, 121.30, 114.94, 114.31, 78.48, 55.51, 48.72, 38.82, 20.56. MS (ESI) for $C_{25}H_{22}N_2O_3$ $[M + H]^+$, calcd: 399,1673 , found: 399,1675.

*4.3.4.9. 10-((3-(4-chlorophenyl)-4,5-dihydroisoxazol-5-yl) methyl)-2-methylacridin-9(10H)-one (**2i**)*. Yellow solid; yield: 67%, mp = 207 °C**.** IR (KBr): 3000, 2985, 1637, 1604, 1591 $cm^{-1}$. $^1H$ NMR (300 MHz, CDCl3, 25 °C, TMS): 8.59 (dd, *J* = 8.1, 1.7 Hz, 1H), 8.37 (s, 1H, H8), 7.72 (td, *J* = 8.8, 6.9, 1.8 Hz, 1H), 7.66–7.45 (m, 5H), 7.45–7.38 (m, 2H), 7.35–7.27 (m, 1H), 5.51–5.31 (m, 1H), 4.76 (dd, *J* = 16.4, 7.4 Hz, 1H), 4.58 (dd, *J* = 16.4, 4.6 Hz, 1H), 3.51 (dd, *J* = 16.7, 7.1 Hz, 1H), 3.23 (dd, *J* = 16.7, 7.1 Hz, 1H), 2.48 (s, 3H, $CH_3$).$^{13}C$ NMR (75 MHz, CDCl3, 25 °C, TMS): 177.79, 156.09, 142.08, 140.29, 136.64, 135.47, 133.89, 131.55, 129.16, 128.12, 128.04, 127.40, 127.31, 122.46, 122.43, 121.53, 114.81, 114.70, 79.10, 48.47, 38.24, 20.54. MS (ESI) for $C_{24}H_{19}ClN_2O_2$ $[M + H]^+$, calcd: 403,1118, found: 403.1117.

*4.3.4.10. 2-methyl-10-((3-(4-nitrophenyl)-4,5-dihydroisoxazol-5-yl)methyl)acridin-9(10H)-one (**2j**)*. Yellow solid; yield: 80%, mp = 220 °C**.** IR (KBr): 3000, 2970, 1638, 1600, 1598 $cm^{-1}$. $^1H$ NMR (300 MHz, DMSO $d_6$, 25 °C, TMS): 8.40 (dd, *J* = 8.0, 1.5 Hz, 1H), 8.33–8.25 (m, 2H), 8.19 (s, 1H), 8.15–8.07 (m, 2H), 7.96–7.75 (m, 3H), 7.68 (dd, *J* = 8.9, 2.3 Hz, 1H), 7.38 (td, *J* = 7.9, 6.3, 1.5 Hz, 1H), 5.42–5.31 (m, 1H), 4.67 (dd, *J* = 15.4, 7.6 Hz, 1H), 4.57 (dd, *J* = 16.3, 4.5 Hz, 1H), 3.84 (dd, *J* = 16.7, 7.1 Hz, 1H), 3.43 (dd, *J* = 16.7, 7.1 Hz, 1H), 2.45 (s, 3H, $CH_3$). $^{13}C$ NMR (75 MHz, DMSO $d_6$, 25 °C, TMS): 176.54, 169.70, 160.62, 148.35, 141.59, 139.83, 135.67, 134.23, 134.11, 131.12, 127.95, 126.79, 126.02, 124.19, 121.77, 121.59, 115.94, 115.76, 79.92,

49.97, 39.54, 20.64. MS (ESI) for $C_{24}H_{19}N_3O_4$ $[M + H]^+$, calcd: 414,1440, found: 414,1431.

*4.3.4.11. 10-((3-(4-(dimethylamino)phenyl)-4,5-dihydroisoxazol-5-yl)methyl)-2-methylacridin-9(10H)-one (**2k**).* White solid; yield: 64%, mp = 141 °C**.** IR (KBr): 3004, 2975, 1639, 1604, 1591 $cm^{-1}$. $^1H$ NMR (300 MHz, CDCl3, 25 °C, TMS): 8.60 (dd, $J$ = 8.0, 1.5 Hz, 1H, H1), 8.39 (s, 1H, H8), 7.86–7.66 (m, 2H), 7.67–7.44 (m, 4H), 7.32 (d, $J$ = 6.6 Hz, 1H), 7.05 (dd, $J$ = 8.5, 6.4 Hz, 1H), 6.71 (d, $J$ = 8.6 Hz, 1H), 5.31 (m, 1H), 4.73 (dd, $J$ = 16.2, 7.3 Hz, 1H), 4.54 (dd, $J$ = 16.3 Hz, 1H), 3.59–3.42 (m, 1H), 3.31–3.17 (m, 1H), 3.05 (s, 6H, CH3), 2.49 (s, 3H, $CH_3$). $^{13}C$ NMR (75 MHz, CDCl3, 25 °C, TMS): 177.84, 156.98, 151.76, 142.14, 140.44, 135.47, 133.86, 129.31, 128.18, 128.02, 127.29, 126.02, 122.44, 121.42, 114.93, 111.72, 78.80, 48.70, 40.12, 20.56. MS (ESI) for $C_{26}H_{25}N_3O_2$, $[M + H]^+$, calcd: 412,1939, found: 412.1938.

*4.3.4.12. 10-((3-(4-hydroxy-3-methoxyphenyl)-4,5-dihydroisoxazol-5-yl)methyl)-2-methylacridin-9(10H)-one (**2l**).* Yellow solid; yield: 65%, mp = 205 °C**.** IR (KBr): 3420, 3014, 2970, 1638, 1603, 1595 $cm^{-1}$ $^1H$ NMR (300 MHz, DMSO $d_6$, 25 °C, TMS): 9.50 (s, 1H, OH), 8.41 (dd, $J$ = 8.1, 1.7 Hz, 1H), 7.78 (d, $J$ = 1.9 Hz, 1H), 7.48–7.41 (m, 1H), 7.33–7.27 (m, 2H), 7.24 (d, $J$ = 8.4 Hz, 1H), 7.22–7.12 (m, 2H), 6.82 (td, $J$ = 7.5, 1.5 Hz, 2H), 5.36 (m, 1H), 4.78 (dd, $J$ = 16.1, 7.5 Hz, 1H), 4.67–4.43 (dd, $J$ = 16.1, 7.5 Hz, 1H), 3.88 (s, 3H, $OCH_3$), 3.53 (dd, $J$ = 17.0, 9.4 Hz, 1H), 3.41–3.1 (dd, $J$ = 17.0, 9.4 Hz, 1H), 2.47 (s, 3H, $CH_3$).$^{13}C$ NMR (75 MHz, DMSO $d_6$, 25 °C, TMS): 178.76, 168.83, 158.04, 148.70, 147.80, 141.36, 140.06, 134.16, 132.19, 131.78, 126.88, 124.21, 123.35, 121.79, 121.64, 121.50, 116.05, 115.83, 114.86, 110.50, 110.12, 79.80, 49.70, 41.12, 20.66. MS (ESI) for $C_{25}H_{22}N_2O_4$ $[M+H]^+$, calcd: 415,1620, found: 415,1622.

## Declaration of Competing Interest

The authors declare that they have no known competing financial interests or personal relationships that could have appeared to influence the work reported in this paper.

## References


Aarjane, M., Aouidate, A., Slassi, S., Amine, A., 2020a. Synthesis, antibacterial evaluation, in silico ADMET and molecular docking studies of new N-acylhydrazone derivatives from acridone. Arab. J. Chem. 13, 6236–6245. https://doi.org/10.1016/j.arabjc.2020.05.034.

Aarjane, M., Slassi, S., Amine, A., 2020b. Novel highly selective and sensitive fluorescent sensor for copper detection based on N-acylhydrazone acridone derivative. J. Mol. Struct. 1199,. https://doi.org/10.1016/j.molstruc.2019.126990 126990.

Aarjane, M., Slassi, S., Tazi, B., Maouloua, M., Amine, A., 2020c. Synthesis, antibacterial evaluation and molecular docking studies of novel series of acridone- 1,2,3-triazole derivatives. Struct. Chem. 31, 1523–1531. https://doi.org/10.1007/s11224-020-01512-0.

Aarjane, M., Slassi, S., Tazi, B., Maouloua, M., Amine, A., 2019. Novel series of acridone-1,2,3-triazole derivatives: microwave-assisted synthesis, DFT study and antibacterial activities. J. Chem. Sci. 131, 85. https://doi.org/10.1007/s12039-019-1653-2.

Alguel, Y., Meng, C., Terán, W., Krell, T., Ramos, J.L., Gallegos, M. T., Zhang, X., 2007. Crystal structures of multidrug binding protein TtgR in complex with antibiotics and plant antimicrobials. J. Mol. Biol. 369, 829–840. https://doi.org/10.1016/j.jmb.2007.03.062.

Amzoiu, M., Amzoiu, D., Belu, I., Popescu, G.-S., Cristea, O.M., Emin, C., Popescu, D.-F., 2020. Comparative study of antibacterial and antifungal activities of acetamidic derivatives. J. Sci. Arts Year.

Banerjee, B., 2017. Recent developments on ultrasound-assisted one-pot multicomponent synthesis of biologically relevant heterocycles. Ultrason. Sonochem. https://doi.org/10.1016/j.ultsonch.2016.10.010.

Bonacorso, H.G., Ketzer, A., Rosa, W.C., Calheiro, T.P., Rodrigues, M.B., Zanatta, N., Martins, M.A.P., Frizzo, C.P., 2018. Useful approach for O-functionalization of trifluoromethyl-substituted spirotetracyclic isoxazolines, and their application in the synthesis of 1,2,3-triazole derivatives. J. Fluor. Chem. 210, 142–148. https://doi.org/10.1016/j.jfluchem.2018.03.012.

Botelho, J., Schulenburg, H., 2020. The role of integrative and conjugative elements in antibiotic resistance evolution. Trends Microbiol. https://doi.org/10.1016/j.tim.2020.05.011.

Brogi, S., Ramalho, T.C., Kuca, K., Medina-Franco, J.L., Valko, M., 2020. Editorial: in silico methods for drug design and discovery. Front. Chem. 8. https://doi.org/10.3389/fchem.2020.00612.

Choudhury, 2010. Molecular docking studies on the activity of naturally occurring pyranochalcones on the transcriptional regulator enzyme of Pseudomonas putida. Open Access Bioinformatics 61. https://doi.org/10.2147/oab.s10901.

Dadiboyena, S., Nefzi, A., 2012. Solid phase synthesis of isoxazole and isoxazoline-carboxamides via [2+3]-dipolar cycloaddition using resin-bound alkynes or alkenes. Tetrahedron Lett. 53, 2096–2099. https://doi.org/10.1016/j.tetlet.2012.02.041.

Daniels, C., Daddaoua, A., Lu, D., Zhang, X., Ramos, J.-L., 2010. Domain Cross-talk during Effector Binding to the Multidrug Binding TTGR Regulator *. https://doi.org/10.1074/jbc.M110.113282.

Drug Likeness Tool (DruLiTo 1) [WWW Document], n.d. URL http://www.niper.gov.in/pi_dev_tools/DruLiToWeb/DruLiTo_index.html (accessed 7.20.20).

Evans, C.E., Matarlo, J.S., Tonge, P.J., Tan, D.S., 2016. Stereoselective synthesis, docking, and biological evaluation of difluoroindanediol-based MenE inhibitors as antibiotics. Org. Lett. https://doi.org/10.1021/acs.orglett.6b03272.

Fahim, A.M., Farag, A.M., 2020. Synthesis, antimicrobial evaluation, molecular docking and theoretical calculations of novel pyrazolo [1,5-a]pyrimidine derivatives. J. Mol. Struct. 1199,. https://doi.org/10.1016/j.molstruc.2019.127025 127025.

Fernandez-Escamilla, A.M., Fernandez-Ballester, G., Morel, B., Casares-Atienza, S., Ramos, J.L., 2015. Molecular binding mechanism of TtgR repressor to antibiotics and antimicrobials. PLoS One 10. https://doi.org/10.1371/journal.pone.0138469.

Franchini, S., Manasieva, L.I., Sorbi, C., Battisti, U.M., Fossa, P., Cichero, E., Denora, N., Iacobazzi, R.M., Cilia, A., Pirona, L., Ronsisvalle, S., Aricò, G., Brasili, L., 2017. Synthesis, biological evaluation and molecular modeling of 1-oxa-4-thiaspiro- and 1,4-dithiaspiro[4.5]decane derivatives as potent and selective 5-HT1Areceptor agonists. Eur. J. Med. Chem. 125, 435–452. https://doi.org/10.1016/j.ejmech.2016.09.050.

Ghaleb, A., Aouidate, A., Ayouchia, H.B. El, Aarjane, M., Anane, H., Stiriba, S.-E., 2020. In silico molecular investigations of pyridine N-Oxide compounds as potential inhibitors of SARS-CoV-2: 3D QSAR, molecular docking modeling, and ADMET screening. J. Biomol. Struct. Dyn. 1–11. https://doi.org/10.1080/07391102.2020.1808530.

Ghaleb, A., Aouidate, A., Bouachrine, M., Lakhlifi, T., Sbai, A., 2019. In silico exploration of aryl halides analogues as CheckpointKinase 1 inhibitors by using 3D QSAR, molecular docking study, and ADMET screening. Adv. Pharm. Bull. 9, 84–92.

Guariento, S., Tonelli, M., Espinoza, S., Gerasimov, A.S., Gainetdinov, R.R., Cichero, E., 2018. Rational design, chemical synthesis and biological evaluation of novel biguanides exploring species-

specificity responsiveness of TAAR1 agonists. Eur. J. Med. Chem. 146, 171–184. https://doi.org/10.1016/j.ejmech.2018.01.059.

Hanwell, M.D., Curtis, D.E., Lonie, D.C., Vandermeerschd, T., Zurek, E., Hutchison, G.R., 2012. Avogadro: An advanced semantic chemical editor, visualization, and analysis platform. J. Cheminform. 4, 17. https://doi.org/10.1186/1758-2946-4-17.

Jia, H., Yu, J., Du, X., Cherukupalli, S., Zhan, P., Liu, X., 2020. Design, diversity-oriented synthesis and biological evaluation of novel heterocycle derivatives as non-nucleoside HBV capsid protein inhibitors. Eur. J. Med. Chem. 112495. https://doi.org/10.1016/j.ejmech.2020.112495.

Kaur, K., Kumar, V., Sharma, A.K., Gupta, G.K., 2014. Isoxazoline containing natural products as anticancer agents: A review. Eur. J. Med. Chem. https://doi.org/10.1016/j.ejmech.2014.02.063.

Kumar, A., Srivastava, K., Raja Kumar, S., Puri, S.K., Chauhan, P. M.S., 2009. Synthesis of 9-anilinoacridine triazines as new class of hybrid antimalarial agents. Bioorganic Med. Chem. Lett. 19, 6996–6999. https://doi.org/10.1016/j.bmcl.2009.10.010.

Li, H.J., Li, X., Liu, N., Zhang, H., Truglio, J.J., Mishra, S., Kisker, C., Garcia-Diaz, M., Tonge, P.J., 2011. Mechanism of the intramolecular claisen condensation reaction catalyzed by MenB, a crotonase superfamily member. Biochemistry 50, 9532–9544. https://doi.org/10.1021/bi200877x.

Mahmoud, W.H., Mahmoud, N.F., Mohamed, G.G., 2017. Synthesis, physicochemical characterization, geometric structure and molecular docking of new biologically active ferrocene based Schiff base ligand with transition metal ions. Appl. Organomet. Chem. 31,. https://doi.org/10.1002/aoc.3858 e3858.

Morris, G.M., Goodsell, D.S., Halliday, R.S., Huey, R., Hart, W.E., Belew, R.K., Olson, A.J., 1998. Automated docking using a Lamarckian genetic algorithm and an empirical binding free energy function. J. Comput. Chem. 19, 1639–1662.

Naouri, A., Djemoui, A., Ouahrani, M.R., Lahrech, M.B., Lemouari, N., Rocha, D.H.A., Albuquerque, H., Mendes, R.F., Almeida Paz, F.A., Helguero, L.A., Bachari, K., Talhi, O., Silva, A.M.S., 2020. Multicomponent and 1,3-dipolar cycloaddition synthesis of triazole- and isoxazole-acridinedione/xanthenedione heterocyclic hybrids: Cytotoxic effects on human cancer cells. J. Mol. Struct. 1217,. https://doi.org/10.1016/j.molstruc.2020.128325 128325.

Oyedele, A.S., Bogan, D.N., Okoro, C.O., 2020. Synthesis, biological evaluation and virtual screening of some acridone derivatives as potential anticancer agents. Bioorganic Med. Chem. 28,. https://doi.org/10.1016/j.bmc.2020.115426 115426.

Paul, S.B., Choudhury, S., 2010. Computational analysis of the activity of pongachalcone I against highly resistant bacteria Pseudomonas putida. Bioinformation 4, 473–477. https://doi.org/10.6026/97320630004473.

Pires, D.E.V., Blundell, T.L., Ascher, D.B., 2015. pkCSM: Predicting small-molecule pharmacokinetic and toxicity properties using graph-based signatures. J. Med. Chem. 58, 4066–4072. https://doi.org/10.1021/acs.jmedchem.5b00104.

Ragusa, G., Gómez-Cañas, M., Morales, P., Rodríguez-Cueto, C., Pazos, M.R., Asproni, B., Cichero, E., Fossa, P., Pinna, G.A., Jagerovic, N., Fernández-Ruiz, J., Murineddu, G., 2017. New pyridazinone-4-carboxamides as new cannabinoid receptor type-2 inverse agonists: Synthesis, pharmacological data and molecular docking. Eur. J. Med. Chem. 127, 398–412. https://doi.org/10.1016/j.ejmech.2017.01.002.

Ribeiro, C.J.A., Nunes, R.C., Amaral, J.D., Gonçalves, L.M., Rodrigues, C.M.P., Moreira, R., Santos, M.M.M., 2017. Spirotriazoline oxindoles: A novel chemical scaffold with in vitro anticancer properties. Eur. J. Med. Chem. 140, 494–509. https://doi.org/10.1016/j.ejmech.2017.09.037.

Righetti, G., Casale, M., Tonelli, M., Liessi, N., Fossa, P., Pedemonte, N., Millo, E., Cichero, E., 2020. New insights into the binding features of F508del CFTR potentiators: a molecular docking, pharmacophore mapping and QSAR analysis approach. Pharmaceuticals 13, 445. https://doi.org/10.3390/ph13120445.

Rouf, A., Şahin, E., Tanyeli, C., 2017. Divergent synthesis of polysubstituted isoxazoles, isoxazoline N-oxides, and dihydroisoxazoles by a one-pot cascade reaction. Tetrahedron 73, 331–337. https://doi.org/10.1016/j.tet.2016.12.005.

Sharma, V., Suvarna, K., Meganathan, R., Hudspeth, M.E.S., 1992. Menaquinone (vitamin K2) biosynthesis: Nucleotide sequence and expression of the menB gene from Escherichia coli. J. Bacteriol. 174, 5057–5062. https://doi.org/10.1128/jb.174.15.5057-5062.1992.

Shirgahi Talari, F., Bagherzadeh, K., Golestanian, S., Jarstfer, M., Amanlou, M., 2015. Potent human telomerase inhibitors: molecular dynamic simulations, multiple pharmacophore-based virtual screening, and biochemical assays. J. Chem. Inf. Model. 55, 2596–2610. https://doi.org/10.1021/acs.jcim.5b00336.

Smith, P., Finnegan, W., Ngo, T., Kronvall, G., 2018. Influence of incubation temperature and time on the precision of MIC and disc diffusion antimicrobial susceptibility test data. Aquaculture 490, 19–24. https://doi.org/10.1016/j.aquaculture.2018.02.020.

Sondhi, S.M., Singh, J., Rani, R., Gupta, P.P., Agrawal, S.K., Saxena, A.K., 2010. Synthesis, anti-inflammatory and anticancer activity evaluation of some novel acridine derivatives. Eur. J. Med. Chem. 45, 555–563. https://doi.org/10.1016/j.ejmech.2009.10.042.

Srivastava, S., Bajpai, L.K., Batra, S., Bhaduri, A.P., Maikhuri, J.P., Gupta, G., Dhar, J.D., 1999. In search of new chemical entities with spermicidal and anti-HIV activities. Bioorganic Med. Chem. 7, 2607–2613. https://doi.org/10.1016/S0968-0896(99)00188-1.

Terán, W., Felipe, A., Segura, A., Rojas, A., Ramos, J.L., Gallegos, M.T., 2003. Antibiotic-dependent induction of Pseudomonas putida DOT-T1E TtgABC efflux pump is mediated by the drug binding repressor TtgR. Antimicrob. Agents Chemother. 47, 3067–3072. https://doi.org/10.1128/AAC.47.10.3067-3072.2003.

Veiga, A., Toledo, M.da.G.T., Rossa, L.S., Mengarda, M., Stofella, N. C.F., Oliveira, L.J., Gonçalves, A.G., Murakami, F.S., 2019. Colorimetric microdilution assay: Validation of a standard method for determination of MIC, IC50%, and IC90% of antimicrobial compounds. J. Microbiol. Methods 162, 50–61. https://doi.org/10.1016/j.mimet.2019.05.003.

Yin, H., Li, G., Chen, X., Wang, W., Wong, P.K., Zhao, H., An, T., 2020. Accelerated evolution of bacterial antibiotic resistance through early emerged stress responses driven by photocatalytic oxidation. Appl. Catal. B Environ. 269,. https://doi.org/10.1016/j.apcatb.2020.118829 118829.

Zghab, I., Trimeche, B., Mansour, M. Ben, Hassine, M., Touboul, D., Jannet, H. Ben, 2017. Regiospecific synthesis, antibacterial and anticoagulant activities of novel isoxazoline chromene derivatives. Arab. J. Chem. 10, S2651–S2658. https://doi.org/10.1016/j.arabjc.2013.10.008.

Zhang, K., Wu, G., Tang, H., Hu, C., Shi, T., Xu, P., 2017. Structural basis for the transcriptional repressor NicR2 in nicotine degradation from *P seudomonas*. Mol. Microbiol. 103, 165–180. https://doi.org/10.1111/mmi.13548.

Zorina, A.D., Nikiforova, N.S., Zarubaev, V.V., Marchenko, S.A., Selivanov, S.I., Starova, G.L., Mehtiev, A.R., Rodionov, E.I., Rodionova, A.A., Trifonov, R.E., 2019. Synthesis, structure and in vitro biological evaluation of new lupane and dammarane triterpenoids fused with pyrazine heterocycle. Mendeleev Commun. 29, 500–502. https://doi.org/10.1016/j.mencom.2019.09.007.